

# CROSS-CALIBRATION OF THREE ELECTRON CLOUD DENSITY DETECTORS AT CESRTA \*

J.P. Sikora<sup>†</sup>, J.R. Calvey, J.A. Crittenden, CLASSE, Ithaca, New York, USA

## Abstract

Measurements of electron cloud density using three detector types are compared under the same beam conditions at the same location in the Cornell Electron Storage Ring (CESR). Two of the detectors sample the flux of cloud electrons incident on the beam-pipe wall. The Retarding Field Analyzer (RFA) records the time-averaged charge flux and has a retarding grid that can be biased to select high energy electrons. The Shielded Button Electrode (SBE) samples the electron flux without a retarding grid, acquiring signals with sub-nanosecond resolution. The third detector uses resonant microwaves and measures the electron cloud density within the beam-pipe through the cloud-induced shift in resonant frequency. The analysis will include comparison of the output from POSINST and E-CLOUD simulations of electron cloud buildup. These time-sliced particle-in-cell 2D modeling codes – simulating photoelectron production, secondary emission and cloud dynamics – have been expanded to include the electron acceptance of the RFA and SBE detectors in order to model the measured signals. The measurements were made at the CESR storage ring, which has been reconfigured as a test accelerator (CESRTA) providing electron or positron beams ranging in energy from 2 GeV to 5 GeV.

## INTRODUCTION

The Cornell Electron Storage Ring (CESR) has a circumference of 768 m and supports positron or electron beams with energies from 2 GeV to 5 GeV. Bunch populations can be as high as  $1.6 \times 10^{11}$  particles/bunch (10 mA/bunch) with total beam populations of  $3.8 \times 10^{12}$  particles/beam. The storage ring has been used as part of a test accelerator program (CESRTA) that includes the measurement of electron cloud (EC) density and mitigation techniques. A number of devices have been installed for EC density measurements at the locations shown in Fig. 1.

The subject of this paper is a comparison of the measurements made with different devices at the same location. Section 15E, shown in Fig. 2, includes a retarding field analyzer (RFA), a shielded button electrode (SBE) and connections for resonant microwave measurements. The RFA and the SBE sample the flux of electrons onto the wall of the beam-pipe, while resonant microwaves are sensitive to the EC density within the beam-pipe volume.

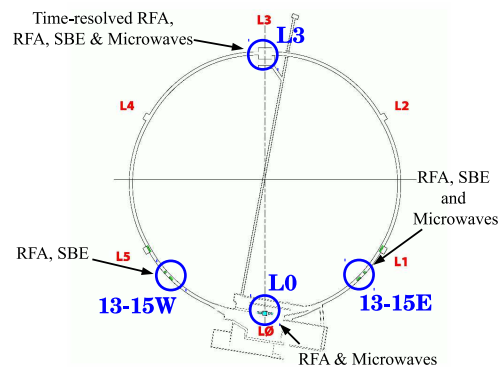


Figure 1: This sketch of the CESRTA storage ring shows the location of electron cloud detectors, including the group at 15E used in this study.

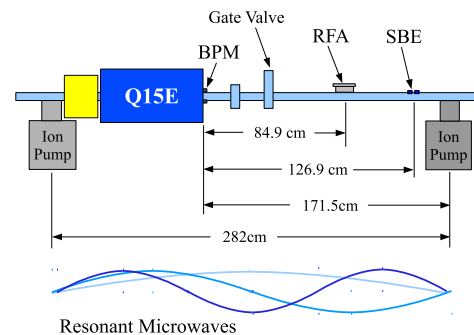


Figure 2: The 15E section of the CESR storage ring contains an SBE, an RFA and a resonant section of beam-pipe.

## RETARDING FIELD ANALYZER

Figure 3 shows the conceptual layout of the RFA [1]. Cloud electrons can enter the detector through an array of small holes in the beam-pipe wall. Nine positively biased collectors are arranged horizontally. The current is time averaged to give a DC current measurement. There is a grid between the holes and the collectors which can be negatively biased to prevent lower energy electrons from impacting the collectors. In a typical measurement, the currents are measured as a function of the grid bias voltage in order to gain information about the energy distribution of the cloud electrons. A plot of such a measurement is given in Fig. 4 showing that most of the electrons are of relatively low energy, but there are some electrons at the central collectors with energies above 200 eV.

## SHIELDED BUTTON ELECTRODE

The SBE also has a pattern of holes that allow electrons to enter the detector, shown in Fig. 5, but the collector provides

\* This work is supported by the US National Science Foundation PHY-0734867, PHY-1002467 and the US Department of Energy DE-FC02-08ER41538, DE-SC0006505.

<sup>†</sup> jps13@cornell.edu

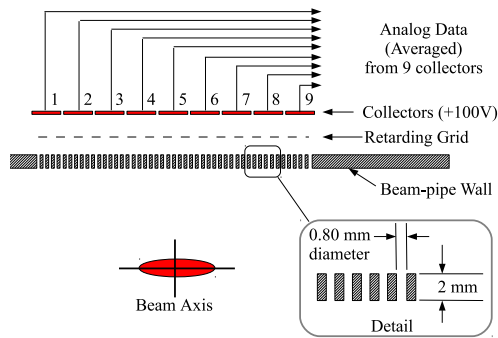


Figure 3: An array of holes in the beam-pipe wall allows cloud electrons to enter the detector. A retarding grid can be biased to suppress electrons with energies below the bias voltage. The array of collectors is arranged horizontally to record the transverse dependence of the current.

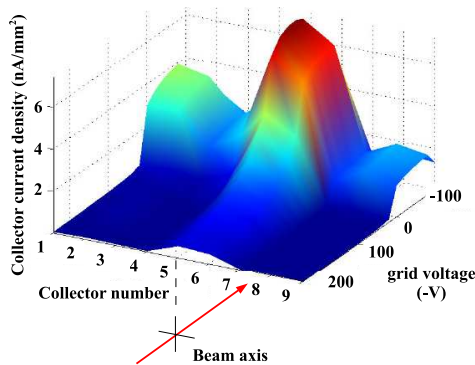


Figure 4: Data from the RFA shows the current versus transverse position for values of the retarding voltage from -100 to 200V. The beam is a 45-bunch train of 5.3 GeV positrons with 14 ns spacing at 1.25 mA/bunch. Collector 1 is toward the outside of the ring.

time-resolved measurements [2, 3]. The collector is of the same design as the buttons used in the beam position monitor (BPM) system, except that it is located behind the array of holes. The depth to diameter ratio of 3:1 (used for both the SBE and the RFA) is effective in suppressing the direct beam signal. The collector is biased at +50 V and the signal is capacitively coupled to +20 dB of amplification and a digital oscilloscope.

Figure 6 shows data from the SBE with two equally populated bunches of 5.3 GeV positrons spaced at 28 ns. The signal from the first bunch comes primarily from photo-electrons since the 2562 ns revolution time of the storage ring is long compared to the lifetime of the electron cloud. The arrival of the second bunch produces a signal from the photo-electrons, but also accelerates into the detector some of the electron cloud produced by the first bunch.

### SIMULATION CODES

Two simulation codes are used in the analysis of data taken with these devices. Both are particle-in-cell time-sliced

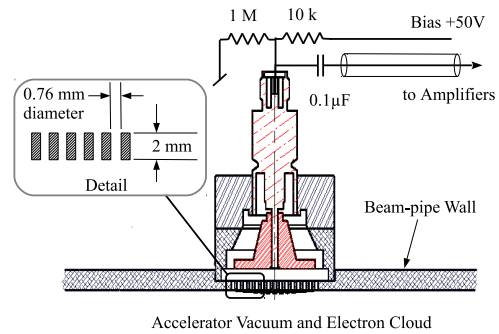


Figure 5: The SBE also has an array of holes that allow electrons to enter the detector. There is no retarding grid and the collector is biased at +50 V.

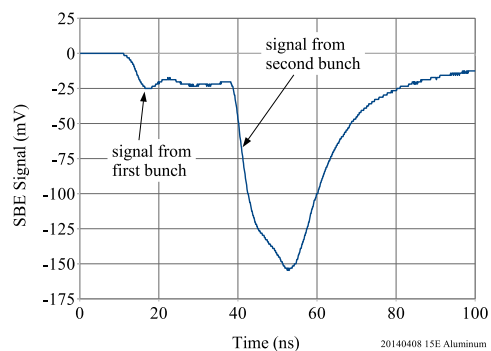


Figure 6: Data from the SBE with two bunches of 5.3 GeV positrons at 3 mA/bunch ( $4.8 \times 10^{10} e^+$ /bunch) spaced by 28 ns.

codes that model the buildup of the electron cloud. The models include the simulation of photo-electron generation, the effect of electrostatic fields by the beam and the cloud, as well as detailed modeling of the interaction of the electrons with the vacuum surface.

The POSINST simulation code [4] was developed at Lawrence Berkeley National Laboratory (LBNL) and the Stanford Linear Accelerator (SLAC) beginning in the 1990s. It has been used in understanding EC effects in PEP-II at SLAC, the Large Hadron Collider (LHC) at CERN and the Advanced Photon Source at Argonne National Laboratory as well as in the design of the damping ring for the International Linear Collider (ILC) [5–7]. The parameters of POSINST are used in fitting the EC buildup model to the data measured with the RFA [8]. This requires that the detector response is included in the model.

The ELOUD code [9] was developed at CERN in the 1990s for simulating EC buildup at the CERN LHC, SPS, and PS. It has also been used at CESR/TA [3, 10] and in the design of the ILC damping ring [7]. The parameters of ELOUD are used in fitting the EC buildup model to the data measured with the SBE. A model of the SBE detector response is included when matching the modeled signal to the data.

Both simulation codes require as input the synchrotron radiation photon rate and absorption site distribution on the vacuum chamber wall. We have used the simulation code SYNRAD [11] to calculate photon rates based on the CESR lattice and ring geometry. In addition, we used the SYN-RAD3D [12] code to obtain the photo-electron production site distribution, since it includes beam-photon tracking, absorption, and scattering on the beam-pipe wall, both diffuse and specular, based on beam-pipe geometry and surface roughness parameters.

An important difference between the ECLLOUD and POSINST codes is in the algorithm for generating secondary electrons. In ECLLOUD, each macroparticle-wall collision produces a single secondary macroparticle, whose charge is scaled by the secondary yield. In POSINST, each collision can generate up to nine secondary macroparticles (depending on the secondary yield), each with its own energy and emission angle. Another difference between the codes is that ECLLOUD provides for different quantum efficiency values for scattered and unscattered photons.

### RESONANT MICROWAVES

An alternate technique for measuring EC density is the use of resonant microwaves [13–15]. When microwaves are coupled into the beam-pipe the response will often be resonant, especially near the cutoff frequency of the beam-pipe. At 15E, reflections produced by the longitudinal slots at two ion pumps generate standing waves between them. Microwaves are coupled into and out of the beam-pipe using the buttons of a BPM between these pumps. The resonant response is shown in Fig. 7. An EC density within the beam-pipe will shift the resonant frequencies slightly, as given by Eq. 1.

$$\frac{\Delta\omega}{\omega_0} \approx \frac{e^2}{2\epsilon_0 m_e \omega_0^2} \frac{\int_V n_e E_0^2 dV}{\int_V E_0^2 dV} \quad (1)$$

With a short train of bunches in the storage ring, this shift will be periodic. With a fixed drive frequency near resonance, the periodic shift in resonant frequency will produce phase modulation sidebands at the revolution frequency above and below the drive frequency. A sketch of the measurement setup is shown in Fig. 8. In the case of 15E, five of the numbered resonances of Fig. 7 are excited and the phase modulation sidebands are measured for each resonance.

### MEASURING EC DENSITY

Each of these techniques has challenges in obtaining an absolute EC density from the measured data. The signals from the RFA and SBE do not have a simple relation to the EC density, so modeling is necessary to infer the density from the measurements.

There are many physical parameters in the ECLLOUD and POSINST simulations that are used for the SBE and RFA respectively. These include the photon distribution, quantum

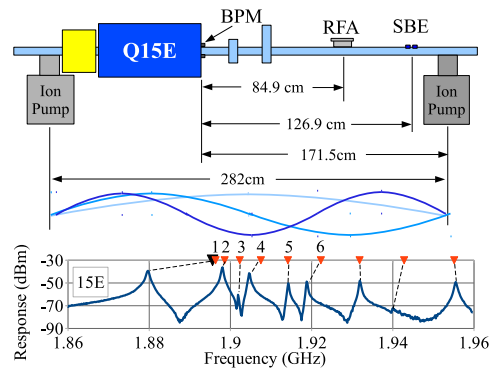


Figure 7: At 15E, reflections from the longitudinal slots at two ion pumps generate a resonant response when the beam-pipe is driven with microwaves at the BPM between them. The five labelled resonances are used in the measurement of EC density.

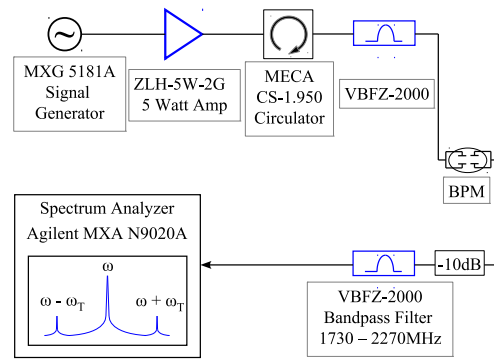


Figure 8: This sketch shows the configuration of instruments used in making resonant microwave measurements.

efficiency, secondary yield as a function of energy, and the angular and energy distributions of the emitted electrons.

Changes in each parameter affect the simulated signal in ways that have considerable overlap, so that it can be difficult to optimize individual parameters. As shown in the Fig. 9 and Fig. 10, the optimized model provides an approximate agreement with the measurement. As a result, fitting the simulation parameters to the data is not straightforward.

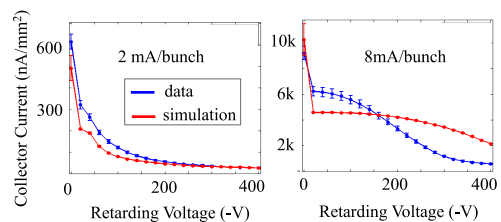


Figure 9: The POSINST simulation output is plotted along with the measured collector currents versus retarding voltage on the RFA. The 8 mA simulation matches the scale of the data, but not the energy distribution.

The microwave measurement of EC density has its own challenges. As described in Ref. [13], a number of steps are

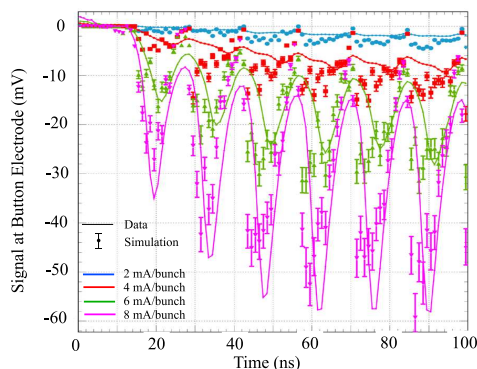


Figure 10: This detail of the ECLLOUD simulation output is plotted along with the measured signal from the SBE. The fit to the measured data looks reasonable at 8 mA/bunch, but at lower bunch currents the simulated signal is larger than the data.

needed to relate an EC density to the measured sideband amplitudes: the EC induced frequency shift becomes a phase shift, but a convolution with the damping time of the resonance is needed; the Fourier components of the resulting phase modulation are calculated with their corresponding modulation sideband amplitudes. In addition to the measured sideband amplitudes, additional measurements or estimates need to be made in order to carry out the calculations: the Q of the resonances, the EC density versus time, and the EC density versus position within the resonant section of beam-pipe [16].

The EC density can vary considerably over the length of the resonant section. While the RFA and the SBE measurements are localized to within a few centimeters of those detectors, the microwave measurement is an average over its length, weighted by  $E^2$ . An estimate for the change in EC density versus position is needed to relate the measurements at the three detectors.

We use the approximation that the EC density will be proportional to the synchrotron radiation photon rate. This ignores the effects of magnetic fields and the possible saturation of the cloud at high photon rates. Figure 11 shows the relative photon rates predicted by SYNRAD for positrons and electrons. The photon rates are normalized to the rate at the longitudinal center of the resonance. Since the RFA and SBE are localized measurements, their values can be scaled by their relative photon rates for comparison. The microwave resonant region and its center are shown at the bottom of the plot, along with the positions of the RFA, SBE and the longitudinal center of the resonance.

This EC density approximation can be used to calculate a correction to the microwave measurements in order to obtain the EC density at the center of the resonant section. If the EC density is either constant or changing linearly along the resonant length, Eq. 1 is unchanged. If the change in EC density is not linear with longitudinal position, a correction is needed. For the 15E resonances, this correction is only a few percent. Once the value at the center of the resonance

has been obtained, it can be scaled to find the EC density values at the RFA and SBE.

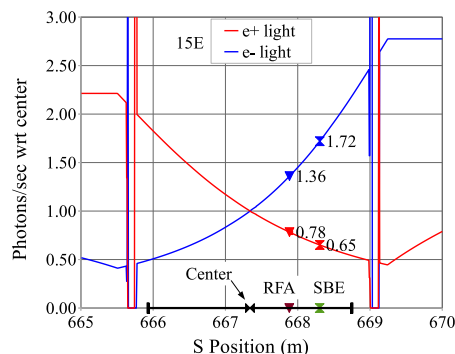


Figure 11: The relative photon rates from positron and electron beams are shown normalized to the rate at the center of the microwave resonance at 15E.

## COMPARISON

For this comparison, data was taken in the 15E aluminum chamber with a 20-bunch train of positrons at 5.3 GeV having bunch currents of 2, 4, 6 and 8 mA (total currents from 40 to 160 mA). At each current step, data was taken with the three detectors.

Using the approximation that the EC density is proportional to the photon rate, the measurements are scaled to the position of the SBE. For the microwave measurements, the EC density versus time from the ECLLOUD simulation is used to calculate the Fourier spectrum.

The EC density versus time for both simulations at 8 mA/bunch is shown in Fig. 12. The growth and decay rates are similar, although the peak EC density from ECLLOUD is lower by about 40%. In Fig. 13 the peak EC densities at four currents are plotted for the simulations and for the microwave measurements. The density derived from the ECLLOUD simulation is lower than the POSINST and microwave values by about 40% over this current range. The densities given by microwave measurements vary depending upon the resonance used over a range that is also about 40%.

## FUTURE WORK

Verification of the models in both the POSINST and ECLLOUD simulations should continue over a wide range of beam energies, bunch populations, magnetic fields and vacuum chamber surfaces. This will ensure that results are applicable to a variety of accelerators and provide robust predictions. Work on resonant microwaves should include improvements in the measurement of Q, the microwave  $E^2$  electric field distribution and the compensation for changes in EC density with position.

## REFERENCES

- [1] J.R. Calvey *et al.*, Nucl. Instrum. Methods Phys. Res., Sect. A **760**, p. 86-97 (2014), <http://dx.doi.org/10.1016/j.nima.2014.05.010>.

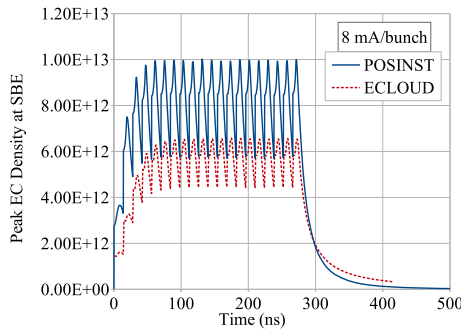


Figure 12: The EC density versus time from POSINST and ECLLOUD at 8 mA/bunch are plotted with both scaled to the location of the SBE.

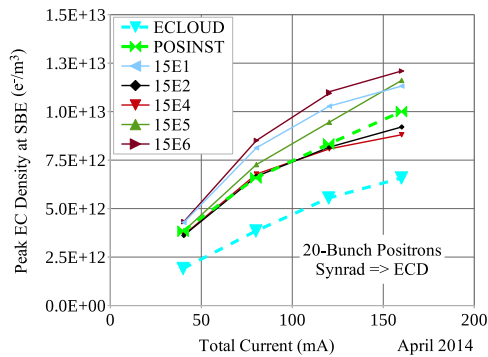


Figure 13: The EC density output from POSINST and ECLLOUD are plotted with microwave measurements for five resonances shown in Fig. 7. All measurements are scaled to the location of the SBE as described in the text.

1016/j.nima.2014.05.051, Preprint, arXiv:1402.7110 [physics.acc-ph].

- [2] J.A. Crittenden *et al.*, Nucl. Instrum. Methods Phys. Res., Sect. A **749**, p. 42-46 (2014), <http://dx.doi.org/10.1016/j.nima.2014.02.047>, Preprint, arXiv:1311.7103 [physics.acc-ph].
- [3] J.A. Crittenden, J.P. Sikora, "Electron Cloud Buildup Characterization Using Shielded Pickup Measurements and Custom Modeling Code at CESRТА," in *Proceedings of ECLLOUD 2012: Joint INFN-CERN-EuCARD-AccNet Workshop on Electron-Cloud Effects, La Biodola, Elba, Italy*, edited by R. Cimino, G. Rumolo, F. Zimmermann, CERN-2013-002, CERN, Geneva, Switzerland, 2013, p. 241-250, arXiv:1307.4013 [physics.acc-ph].
- [4] M.A. Furman, M.T.F. Pivi, "Probabilistic Model for the Simulation of Secondary Electron Emission," Phys. Rev. ST Accel. Beams **5**, 124404 (Dec. 2002).

- [5] M.A. Furman, G.R. Lambertson, "The Electron Cloud Instability in the Arcs of the PEP-II Positron Ring," in *Proceedings of MBI97: International Workshop on Multibunch Instabilities in Future Electron and Positron Accelerators*, Tsukuba, Japan, 1997, Y. H. Chin, Ed. (1997), KEK Proceedings 97-17, p. 170.
- [6] M.A. Furman, "The Electron-Cloud Effect in the Arcs of the LHC," Tech. Rep. LHC Project Report 180/LBNL-41482/CBP Note 247, CERN, Geneva, Switzerland (May 1998).
- [7] J.A. Crittenden *et al.*, "Investigation into Electron Cloud Effects in the International Linear Collider Positron Damping Ring," Phys. Rev. ST Accel. Beams **17**, March 2014, 031002.
- [8] J.R. Calvey *et al.*, "Measurement and Modeling of Electron Cloud in a Field Free Environment Using Retarding Field Analyzers," Phys. Rev. ST Accel. Beams **17**, June 2014, 061001, arXiv:1402.7110.
- [9] F. Zimmermann, G. Rumolo, K. Ohmi, "Electron Cloud Build Up in Machines with Short Bunches," ICFA Beam Dynamics Newsletter **Nr. 33**, eds. K. Ohmi & M. Furman (2004).
- [10] J.A. Crittenden *et al.*, "Progress in Studies of Electron-Cloud-Induced Optics Distortions at CESRТА," in *Proceedings of IPAC10, Kyoto, Japan* (2010).
- [11] D. Sagan, "Design and Applications of the Bmad Library for the Simulation of Particle Beams and X-rays," in *11th International Computational Accelerator Physics Conference, Rostock-Warnemünde, Germany* (2012).
- [12] G.F. Dugan, D. Sagan, "SYNRAD3D Photon Propagation and Scattering Simulations," in *Proceedings of ECLLOUD 2012: Joint INFN-CERN-EuCARD-AccNet Workshop on Electron-Cloud Effects, La Biodola, Elba, Italy*, edited by R. Cimino, G. Rumolo, F. Zimmermann, CERN-2013-002, CERN, Geneva, Switzerland, 2013, p. 117-129.
- [13] J.P. Sikora *et al.*, Nucl. Instrum. Methods Phys. Res., Sect. A **754**, pp. 28-35 (2014), <http://dx.doi.org/10.1016/j.nima.2014.03.063>, Preprint, arXiv:1311.5633 [physics.acc-ph].
- [14] J.P. Sikora *et al.*, "TE Wave Measurement and Modeling," in *Proceedings of ECLLOUD 2012: Joint INFN-CERN-EuCARD-AccNet Workshop on Electron-Cloud Effects, La Biodola, Elba, Italy*, edited by R. Cimino, G. Rumolo, F. Zimmermann, CERN-2013-002, CERN, Geneva, Switzerland, 2013, p. 193-200, arXiv:1307.4315 [physics.acc-ph].
- [15] J.P. Sikora *et al.*, "Resonant TE Wave Measurement of Electron Cloud Density Using Multiple Sidebands," in *Proceedings of IBIC'13, Oxford, United Kingdom, September 2013, TUPF34*, (2013).
- [16] J.P. Sikora *et al.*, "Electron Cloud Density Measurements Using Resonant Microwaves at CESRТА," *these proceedings*, WEPF21, IBIC'14, Monterey, CA, USA (2014).